


Article

One-Pot Synthesis of Ultra-Small Pt Dispersed on Hierarchical Zeolite Nanosheet Surfaces for Mild Hydrodeoxygenation of 4-Propylphenol

Piraya Wetchasat¹, Saros Salakhum^{1,*} , Thidarat Imyen¹, Duangkamon Suttipat¹, Wannaruedee Wannapakdee¹, Marisa Ketkaew¹, Anittha Prasertsab¹, Pinit Kidkhunthod², Thongthai Wittoon³ and Chularat Wattanakit¹

¹ Department of Chemical and Biomolecular Engineering, School of Energy Science and Engineering, Nanocatalysts and Nanomaterials for Sustainable Energy and Environment Research Network of NANOTEC, Vidyasirimedhi Institute of Science and Technology, Rayong 21210, Thailand;

piraya.w_s17@vistec.ac.th (P.W.); thidarat.i@vistec.ac.th (T.I.); s15_duangkamon.s@vistec.ac.th (D.S.); wannaruedee.w@vistec.ac.th (W.W.); marisa.k_s16@vistec.ac.th (M.K.); anittha.p_s19@vistec.ac.th (A.P.); chularat.w@vistec.ac.th (C.W.)

² Synchrotron Light Research Institute (Public Organization), Nakhon Ratchasima 30000, Thailand; pinit@slri.or.th

³ Center of Excellent on Petrochemical and Materials Technology, Department of Chemical Engineering, Faculty of Engineering, Kasetsart University, Bangkok 10900, Thailand; fengttwi@ku.ac.th

* Correspondence: saros.s@vistec.ac.th



Citation: Wetchasat, P.; Salakhum, S.; Imyen, T.; Suttipat, D.; Wannapakdee, W.; Ketkaew, M.; Prasertsab, A.; Kidkhunthod, P.; Wittoon, T.; Wattanakit, C. One-Pot Synthesis of Ultra-Small Pt Dispersed on Hierarchical Zeolite Nanosheet Surfaces for Mild Hydrodeoxygenation of 4-Propylphenol. *Catalysts* **2021**, *11*, 333. <https://doi.org/10.3390/catal11030333>

Academic Editor: Kyungsu Na

Received: 16 February 2021

Accepted: 26 February 2021

Published: 5 March 2021

Publisher's Note: MDPI stays neutral with regard to jurisdictional claims in published maps and institutional affiliations.



Copyright: © 2021 by the authors. Licensee MDPI, Basel, Switzerland. This article is an open access article distributed under the terms and conditions of the Creative Commons Attribution (CC BY) license (<https://creativecommons.org/licenses/by/4.0/>).

Abstract: The rational design of ultra-small metal clusters dispersed on a solid is of crucial importance in modern nanotechnology and catalysis. In this contribution, the concept of catalyst fabrication with a very ultra-small size of platinum nanoparticles supported on a hierarchical zeolite surface via a one-pot hydrothermal system was demonstrated. Combining the zeolite gel with ethylenediaminetetraacetic acid (EDTA) as a ligand precursor during the crystallization process, it allows significant improvement of the metal dispersion on a zeolite support. To illustrate the beneficial effect of ultra-small metal nanoparticles on a hierarchical zeolite surface as a bifunctional catalyst, a very high catalytic performance of almost 100% of cycloalkane product yield can be achieved in the consecutive mild hydrodeoxygenation of 4-propylphenol, which is a lignin-derived model molecule. This instance opens up perspectives to improve the efficiency of a catalyst for the sustainable conversion of biomass-derived compounds to fuels.

Keywords: ultra-small nanoparticles; hierarchical zeolite nanosheets; hydrodeoxygenation

1. Introduction

The rational design of ultra-small metal nanoparticles is one of the most fascinating perspectives in modern nanotechnology because they are of crucial importance in a multiplicity of fields, for instance, adsorption [1], separation [2] to sensor [3], biosensor [4], drug delivery [5], renewable energy [6], photocatalysis [7], and especially industrial catalysis [8]. Previously, although metal nanoparticles (NPs) have been extensively developed and used in many potential catalytic applications, such as Fischer-Tropsch synthesis [9], CO oxidation process [10], hydrogenation [11], hydroisomerization [12], and hydrodeoxygenation [13], they usually suffer from the drawback of metal agglomeration at elevated temperature, eventually leading to the catalytic activity loss during the reaction [14–16]. To circumvent these limitations, various solid materials, such as metal organic frameworks (MOFs), metal oxides, mesoporous silicas, and zeolites have been globally used for dispersing and stabilizing metal nanoparticles, and subsequently improving the dispersion of nanoparticles [17,18]. Among them, a zeolite is the most promising candidate and has been extensively applied in fine-chemical and petrochemical industries owing to their outstanding properties in terms of confinement effect [19], shape selectivity [20], thermal

stability [21], tunable acidity [22], and ion-exchange ability [23]. To date, various transition metals, such as Pt [17,18], Pd [24], Ag [25], Au [26], and Cu [27] have been successfully incorporated into a zeolite framework, exhibiting their unique properties for various catalytic chemical reactions, for example, oxidation, hydrogenation, isomerization, and Fischer-Tropsch synthesis [28]. The use of zeolites for hosting ultra-small nanoparticles benefits the stabilization of metal particles inside zeolite frameworks due to their confinement effect, eventually preventing the metal aggregation when they have been operated at high reaction temperature [29]. In general, there are several proposed approaches for the fabrication of metal nanoparticles and zeolites, such as wet impregnation (IM), ion-exchange, deposition-precipitation (DP), and one-pot hydrothermal synthesis [30]. Although a wet impregnation is a very simple method, which has been traditionally used in the industrial processes, it often suffers from the drawbacks of large and non-homogeneous metal particles that are mostly deposited on the external surface of zeolites due to a relatively weak metal-support interaction [31]. On the other hand, a one-pot synthesis would provide well-dispersed and ultra-small metal clusters on zeolite surfaces, and these particles are resistant to metal sintering [32–39]. Moreover, the leaching of metal nanoparticles from zeolite surfaces can be prevented, eventually improving the stability and reusability of a catalyst. As a result, the catalytic performance in many reactions can be enhanced over the ultra-small metals dispersed on zeolites such as a hydrogenation and tandem aldol condensation [40].

Although there are several benefits (mentioned above) of the encapsulation of metal clusters inside a framework of zeolites, it often suffers from the disadvantage of using a conventional zeolite with a bulk structure. It has been reported that a small microporous structure of the conventional zeolite can suppress the catalytic activity of a reaction involving a bulky molecule [41,42]. In order to overcome these drawbacks, a hierarchical zeolite containing at least two levels of porous structures (micropores with integrated macropores or/and mesopores) has been recently used to enhance the catalytic efficiency because it improves the transportation of bulky compounds into active sites as well as promotes the metal dispersion on solid zeolites [43]. Indeed, there are a lot of efforts to develop the synthesis approaches of hierarchically structured zeolites. One of the most interesting approaches is using the soft templating method with the aid of various chemical agents, such as hydrophilic cationic polymers [44,45], and organosilanes [46,47]. In particular, the hierarchical zeolite nanosheet, one type of hierarchical zeolites, has played an essential role in the recent years because it not only improves diffusion limitation of bulky molecules in small pores but also enhances metallic sites when using it as a solid support [47–52].

Not only the above-mentioned advantage of using a zeolite framework to stabilize the ultra-small metal nanoparticles, but also the combination of acid zeolite together with the metallic particles would benefit in many catalytic applications because it can be considered as a bifunctional catalyst [53,54]. Typically, there are several catalytic reactions, requiring the presence of a bifunctional Brønsted acid and Lewis acid catalyst, such as hydrocracking [55], hydrogenation [56], and especially hydrodeoxygenation (HDO), which is one of the most crucial pathways in bio-oil upgrading applications [57–59]. It is well known that a very high content of oxygenates in bio-oils has been observed after the pyrolysis of corresponding bio-oils, eventually producing a low quality of liquid fuels [60]. To overcome these problems, the hydrodeoxygenation (HDO) is one of the most effective ways for removal of oxygen parts from bio-oils to increase their quality. Typically, it requires the simultaneous presence of Lewis acid and Brønsted acid sites in an overall HDO process because the former is the main function for hydrogenation reaction and the latter is responsible for dehydration [57]. Therefore, the competence of a catalyst on HDO reaction depends on balancing of these two catalytic functions. For example, the catalytic performance of hydrogenation of lignin-derived compound using bifunctional Pt-Ru/Proton Zeolites Socony Mobil-5 (HZSM-5) nanosheets has been significantly improved because the bimetallic nanoparticles on a zeolite support provide the crucial factor to increase the high dispersibility of two metal species [51]. Moreover, Hidetoshi et al. reported the catalytic conversion of HDO of 4-propylphenol phenol using Pt supported on various zeolites. The Pt/HZSM-5 provided

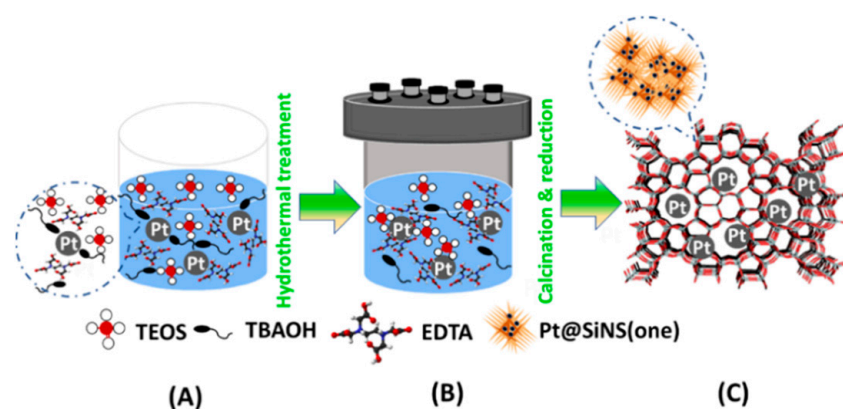
the best catalytic performance, in which almost 100% yield of propylcyclohexane at mild reaction condition was observed [61].

In order to improve the efficiency of above-mentioned bifunctional catalysts, one needs to highly disperse the ultra-small metal nanoparticles, which are located closely to the Brønsted acid site in a zeolite framework. In this contribution, we have successfully fabricated the ultra-small platinum nanoparticles dispersed on hierarchical zeolite surfaces by a one-pot hydrothermal system using the metal stabilization by interacting with ethylenediaminetetraacetic acid (EDTA) as a ligand precursor. In addition, the ultra-small metal nanoparticles on acid zeolite surfaces are advantageous for the mild 4-propylphenol hydrodeoxygenation as a model reaction for bio-oil upgrading application with a very high catalytic performance.

2. Results and Discussion

2.1. Analysis of Structural and Morphological Structures

The present study demonstrates the perspectives of the fabrication of ultra-small Pt nanoparticles (Pt NPs) onto hierarchical zeolite nanosheets by utilizing a polyprotic acid as a chelating agent to effectively stabilize metal ions in zeolite domains during the crystallization via a one-pot hydrothermal synthesis (Scheme 1). It is well known that ethylenediaminetetraacetic acid (EDTA) is one of the most important polyprotic aminocarboxylic acids, which can form metal-ligand complexes with various metals [62,63]. As illustrated in Scheme 1A, EDTA molecules interact with the Pt precursors forming chelated Pt complexes in the synthesis gel, which contains tetraethyl orthosilicate (TEOS) and tetrabutylammonium hydroxide (TBAOH) as a starting silica and a structure-directing agent, respectively. Accordingly, the Pt precursors can be introduced to the zeolite matrix upon the dissolution of silica species followed by the formation of silicate network around the Pt-EDTA complexes under the direction of TBAOH (Scheme 1A). After the crystallization under a hydrothermal condition and the reduction under H₂ atmosphere (Scheme 1B,C), ultra-small Pt nanoparticles dispersed on hierarchical zeolite nanosheet surfaces have been successfully obtained and the sample is denoted as Pt@SiNS(one) or Pt@HZSM-5NS(one) when using silicalite-1 and HZSM-5 as supports, respectively. Moreover, to clarify the effects of the preparation method on the characteristic of Pt nanoparticles, the impregnation method was employed for adding Pt nanoparticles on hierarchical nanosheets and conventional zeolites (denoted as Pt/SiNS(imp) or Pt/HZSM-5(imp), and Pt/SiCON(imp) or Pt/HZSM-5CON(imp), respectively). The Pt content of all the prepared samples corresponds to 0.4–0.6 wt.% (Table S1).



Scheme 1. Illustration of the synthesis step for ultra-small Pt nanoparticles supported on hierarchical silicalite-1 nanosheets: (A) the self-assembly of Pt and EDTA in the presence of silica source (TEOS) and the structure-directing agent (TBAOH), (B) the hydrothermal process of zeolite in the presence of the Pt-EDTA complex, (C) the obtained ultra-small Pt particles dispersed on a zeolite structure.

As shown in Figure 1A, the X-ray diffraction (XRD) patterns of all the prepared samples obviously verify the characteristic of the MFI (pentasil type zeolite) topology without a contamination of other crystalline phases [64,65]. As expected, a lower crystallinity shown by a lower intensity of the diffraction peaks of the zeolite nanosheet samples with respect to the conventional zeolite relates to a smaller crystallite size and a partial loss of micropores, which are typically found in case of hierarchical zeolite nanocrystals [46]. Interestingly, the XRD pattern of Pt@SiNS(one) does not exhibit the peaks referring to metallic Pt (39.8° and 46.2°) [40,66], which can be explained by a low Pt content or a well dispersion of Pt nanoparticles [40]. The scanning electron micrograph (SEM) reveals that both Pt@SiNS(one) and Pt/SiNS(imp) samples exhibit the uniform spherical assemblies of aggregated MFI nanosheets with the particle size of 123.2 ± 11.6 nm and 166.5 ± 18.2 nm (Figure 1B,C and Figure S1), respectively, which are in consistent with what has been illustrated previously [67].

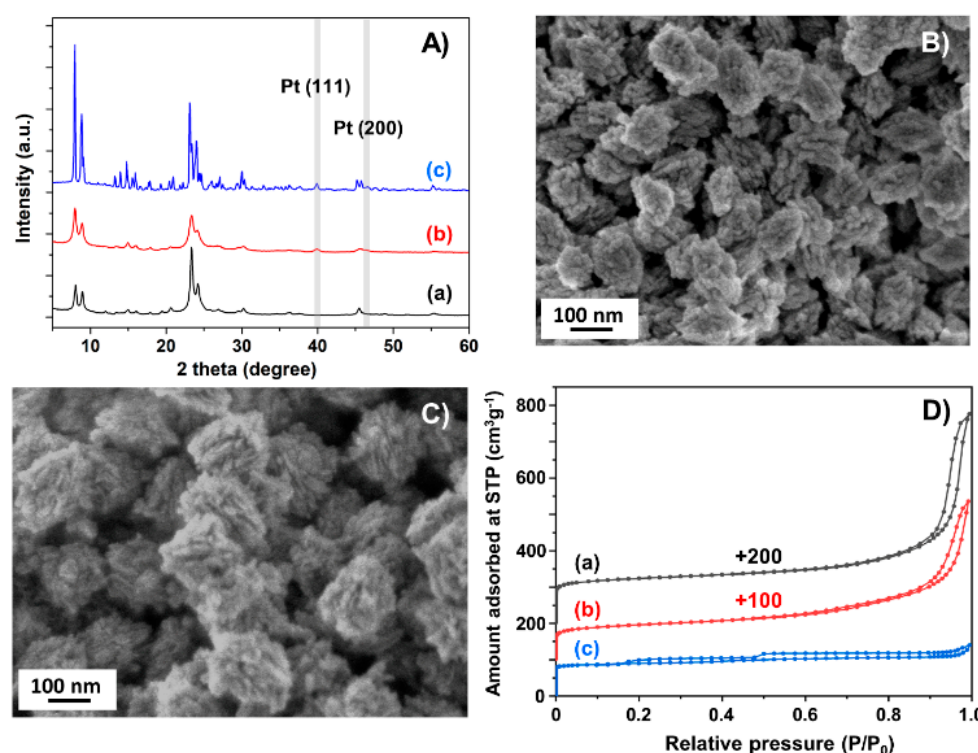


Figure 1. (A) X-ray diffraction (XRD) patterns of (a) Pt@SiNS(one), (b) Pt/SiNS(imp), and (c) Pt/SiCON(imp), scanning electron micrograph (SEM) images of (B) Pt@SiNS(one) and (C) Pt/SiNS(imp), and (D) N₂ adsorption/desorption isotherms of (a) Pt@SiNS(one), (b) Pt/SiNS(imp), and (c) Pt/SiCON(imp).

In strong contrast to this, the Pt/SiCON(imp) exhibits cubic-shaped crystals with the particle size of 1.8 ± 0.1 μm (Figure S1). To gain the insights into the textural properties of all the synthesized materials, N₂ sorption isotherms of all samples and the summarization of textural information are shown in Figure 1D and Table 1, respectively. Typically, the Pt/SiCON(imp) sample displays a type-I isotherm because of the adsorbed filling in a micropores at the low P/P_0 or relative pressure, which is a typical characteristic of a microporous material [68]. However, the different appearance of N₂ sorption isotherms could be investigated for both Pt@SiNS(one) and Pt/SiNS(imp) samples demonstrating the characteristics of combined type-I and type-IV isotherms, as clearly observed by a hysteresis loop at high P/P_0 (above 0.8), corresponding to a capillary condensation in larger meso/macropores [68]. The corresponding textural properties of all the synthesized samples are illustrated in Table S1.

Table 1. Textural properties of the synthesized Pt supported on various silicalite-1 supports prepared by different methods.

Sample	S_{BET} ^[a]	S_{micro} ^[b]	S_{ext} ^[c]	V_{total} ^[d]	V_{micro} ^[e]	V_{ext} ^[f]	$V_{\text{ext}}/V_{\text{total}}$ ^[g]
Pt@SiNS(one)	391	252	139	0.89	0.14	0.75	0.84
Pt/SiNS(imp)	314	171	143	0.68	0.09	0.59	0.87
Pt/SiCON(imp)	284	226	58	0.22	0.11	0.11	0.50

^[a] Brunaur-Emmett-Teller (BET) specific surface area, ^[b] microporous surface area, ^[c] external surface area, ^[d] total pore volume, ^[e] micropore volume, ^[f] external volume = $V_{\text{total}} - V_{\text{micro}}$, and ^[g] fraction of external volume. All surface areas and pore volumes are in the unit of $\text{m}^2 \cdot \text{g}^{-1}$ and $\text{cm}^3 \cdot \text{g}^{-1}$, respectively.

As expected, BET surface area is improved in cases of Pt-loaded silicalite-1 nanosheet samples with respect to Pt/SiCON(imp) due to their enhanced mesoporosity. Interestingly, a lower BET surface area of Pt/SiNS(imp) with respect to Pt@SiNS(one) indicates that Pt nanoparticles in Pt/SiNS(imp) are probably located on the outermost surface of zeolite, eventually blocking the zeolite pore entrances. The high-resolution TEM image of Pt@SiNS(one) reveals the small dark spots dispersing on the zeolite nanosheets surfaces (Figure 2A), likely corresponding to ultra-small Pt nanoparticles deposited on a zeolite matrix. To verify this hypothesis, the STEM-EDS elemental mapping of Pt@SiNS(one) was performed (Figure 2B). The results demonstrate that Pt nanoparticles are homogeneously distributed in the matrix of silicate-1 nanosheets with the average particle size of 1.09 ± 0.22 nm (Figure 2B,C). In strong contrast to this, the Pt/SiNS(imp) prepared by the impregnation method, the agglomeration of Pt nanoparticles is observed with the corresponding average particle size of 3.19 ± 0.52 nm (Figure S2A).

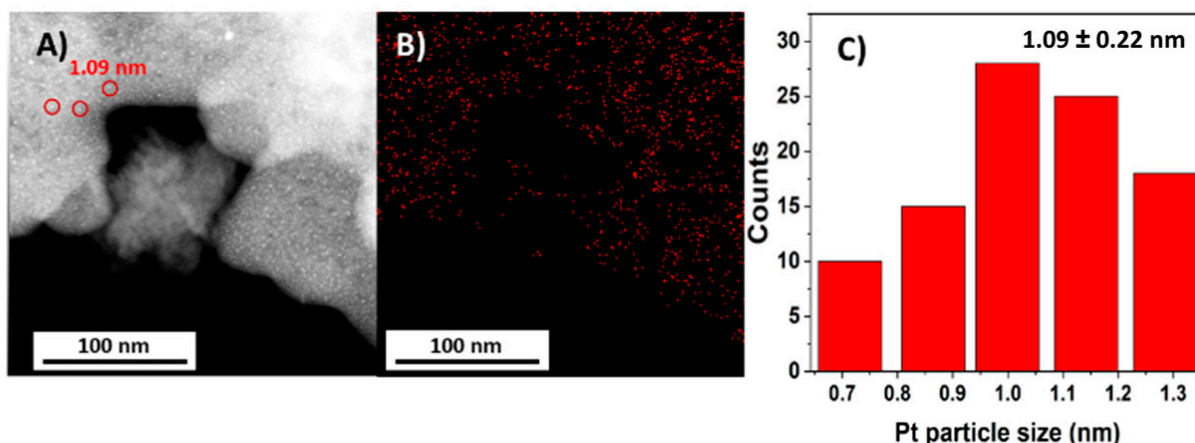


Figure 2. (A) STEM image by high-angle annular dark-field mode (HAADF-STEM), (B) STEM image with EDS mapping for Pt (red dot color represents Pt particles), and (C) Pt particle size distribution of Pt@SiNS(one).

Remarkably, the significantly smaller Pt nanoparticles in Pt@SiNS(one) with respect to Pt/SiNS(imp) relate to the fact that the use of EDTA for Pt incorporation into the zeolite synthesized a one-pot hydrothermal system can effectively control the Pt particle size distribution, subsequently preventing the aggregation of Pt nanoparticles. In addition, in the case of Pt impregnated on the conventional zeolite (Pt/SiCON(imp)), Pt precursor cannot be incorporated inside the micropores, and Pt nanoparticles then tend to agglomerate to large clusters (43.2 ± 0.1 nm) deposited on the external surface of a zeolite (Figure S2B) upon the calcination process [15,69].

Typically, metal-acid bifunctional catalysts are known to be a highly efficient material for hydrodeoxygenation (HDO) process, which is one of the most favourable pathways for the application of bio-oil conversion [51]. Indeed, the key factor to achieve high catalytic performance in the HDO process is the close proximity of the metallic nanoparticles with the Brønsted acid sites of a zeolite [70,71].

Indeed, the improvement of ultra-small metal nanoparticles (<1.5 nm in diameter) deposited onto the zeolite surface is of crucial importance to promote sequential reactions

on two different active sites, and therefore the high catalytic activity would be achieved [71]. Remarkably, the present work demonstrates the successful fabrication of Pt nanoparticles onto the siliceous MFI (silicalite-1) zeolite nanosheet as evidenced above. Consequently, the above-mentioned efficient synthesis approach was further employed to prepare metal-acid bifunctional catalysts, containing the highly dispersed Pt nanoparticles on protonated MFI zeolite nanosheets (denoted as Pt@HZSM-5NS(one)).

To characterize the chemical and physical properties of the metal-acid bifunctional ZSM-5 synthesized by a one-pot synthesis (Pt@HZSM-5NS(one)) with respect to the ones prepared by an impregnation method (referred as Pt/HZSM-5NS(imp) and Pt/HZSM-5CON(imp), for Pt loaded onto H-ZSM-5 nanosheet, and conventional H-ZSM-5, respectively), their crystalline structures, morphologies, textural properties, zeolite particle size distribution, and Pt particle size distribution are presented in Figures S3–S6 and Table S2. XRD patterns again confirm that the MFI topology is the main characteristics without the interference of any crystalline phases (Figure S3A) as well as no characteristic of platinum oxides was observed for Pt@HZSM-5NS(one), whereas Pt/HZSM-5NS(imp) and Pt/HZSM-5CON(imp) show some characteristics of platinum oxides at 2θ of 39.2° , corresponding to the characteristic of Pt nanoparticles [40,62].

The N_2 sorption isotherms again confirm the presence of the combined micro-meso/macroporous structures of Pt@HZSM-5NS(one), and Pt/HZSM-5NS(imp), whereas the Pt/HZSM-5CON(imp) contains the microporous structure as evidenced by the type-I N_2 isotherm (Figure S3B). As for the zeolite particle size and Pt particle size distribution, it was found that the particle sizes of zeolites are in the range of 93.1 ± 9.4 nm, 123.6 ± 17.8 nm, and 6.9 ± 1.1 μ m, and Pt particle sizes are approximately 0.94 ± 0.28 , 5.57 ± 0.40 , and 38.0 ± 0.02 nm for Pt@HZSM-5NS(one), Pt/HZSM-5NS(imp), and Pt/HZSM-5CON(imp), respectively (Figure S4–S6).

The electronic properties and chemical bonding of Pt in the bifunctional catalysts were studied by X-ray absorption near-edge spectroscopy (XANES). As depicted in Figure S7, the normalized Pt L3 edge XANES spectra of all Pt-modified H-ZSM-5 catalysts exhibit the absorption edge feature (E_0) close to that of Pt white line at the L3 edge is increased as Pt foil (11,564 eV) [72], confirming that Pt clusters were fully reduced under H_2 atmosphere. Moreover, the intensity of the white line peak at 11,564 eV related to electronic transitions from $2p_{3/2}$ core level to unoccupied 5d states of all samples is higher than that of Pt foil, presenting the remarkable electronic force between Pt nanoparticles and zeolite support [73]. Typically, the intensity of the white line at the L3 edge is increased as Pt particle size decreases [74,75]. Interestingly, the most intense white line feature of Pt@HZSM-5NS(one) demonstrates that Pt nanoparticles are the smallest and highly dispersed with respect to the other samples, corresponding to the above results.

To investigate the acid properties of the metal-acid bifunctional ZSM-5, the NH_3 -TPD experiments have been performed (Figure S8). According to NH_3 -TPD profiles of all three samples (Pt@HZSM-5NS(one), Pt/HZSM-5NS(imp), and Pt/HZSM-5CON(imp)), two NH_3 desorption peaks at around 180 to 200 $^\circ$ C and 350 to 400 $^\circ$ C, have been obtained corresponding to NH_3 desorption from weak and strong acid locations at low and high temperatures, respectively. Accordingly, the weak and strong acid densities of all the synthesized samples are demonstrated in Table S3. The results show that all three synthesized bifunctional catalysts exhibit a comparable acid density.

2.2. Catalytic Test in Hydrodeoxygenation (HDO) Process

As stated above, the hydrodeoxygenation (HDO) can be performed using the bifunctional catalysts containing the hydrogenation site and acid sites. Typically, hydrogenation occurs on Pt sites and dehydration can be catalyzed by the Brønsted acid sites (Figure 3A,B). As shown in Figure 3A, the hydrodeoxygenation of 4-propylphenol to propylcyclohexane proceeds via multiple steps of a reaction composed of hydrogenation and dehydration. Hence, the bifunctional catalysts containing both Lewis metallic sites (Hydrogenation) and Brønsted acid sites (Dehydration) are needed [76–79]. Therefore, if both active sites are

located closely in the porous network of zeolite, this would be interesting to transfer the intermediates from one to another sites, eventually enhancing the catalytic performance (Figure 3B). In the case of Pt located on the outermost surface of the zeolite crystal as displayed in Figure 3B, the distance between metallic Pt and Brønsted acid sites in zeolite framework is quite far from each other. Hence, in order to complete the hydrodeoxygenation process, the substrate needs to diffuse from Pt sites located on the outermost surface into the microporous network in which Brønsted acid sites are located, and even more it has to diffuse back again to the Pt sites located at the external surface as the last hydrogenation step.

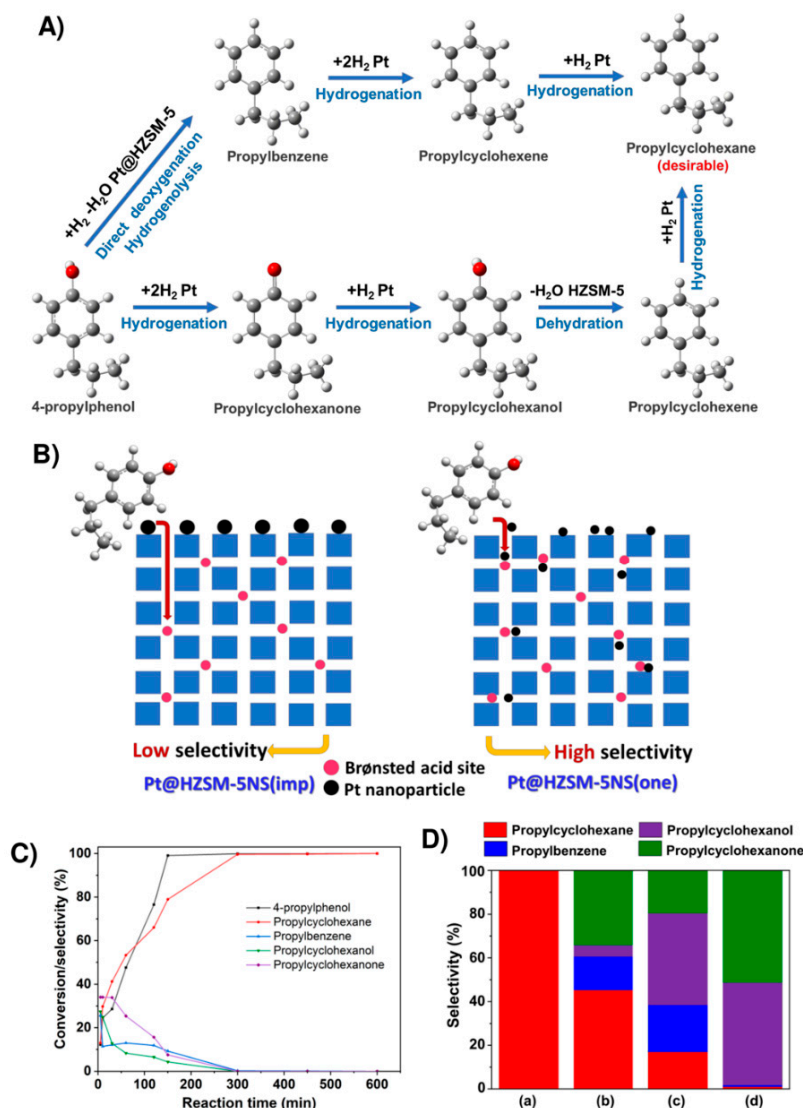


Figure 3. (A) Proposed reaction pathway of the 4-propylphenol conversion to propylcyclohexane over bifunctional Pt supported on an acid catalyst, (B) Illustration of the proposed perspective of 4-propylphenol conversion over Brønsted acid sites and Pt active sites of Pt/HZSM-5NS(imp) and Pt@HZSM-5NS(one), (C) Catalytic behaviors of Pt@HZSM-5NS(one) in the hydrodeoxygenation of 4-propylphenol as shown in terms of reactant conversion (%) and product selectivity (%) as a function of reaction time, and (D) Product selectivity (%) in the hydrodeoxygenation of 4-propylphenol over (a) Pt@HZSM-5NS(one), (b) Pt/HZSM-5NS(imp), (c) Pt/HZSM-5CON(imp), and (d) Pt@NaZSM-5NS(one). The catalytic results were investigated at 110 °C under H₂ atmospheric pressure for 10 h.

To explore the reaction pathway of 4-propylphenol hydrodeoxygenation over the Pt@ZSM-5NS(one) catalyst (Figure 3A), the conversion of 4-propylphenol and product distribution vs. reaction time are demonstrated as shown in Figure 3C. Firstly, 4-propylphenol was transformed to propylcyclohexanone via a partial hydrogenation, and then subsequently further facilitated to propylcyclohexanol. Subsequently, propylcyclohexanol is dehydrated to propylcyclohexene and eventually hydrogenated to propylcyclohexane [51,80,81]. It is reasonable to assume that propylcyclohexene is also produced as an intermediate via direct deoxygenation, which is further hydrogenated to propylcyclohexane [51,80–82]. Interestingly, the conversion of 4-propylphenol reached 99% within 150 min (Figure 3C and Table S4), which is contributed to the effect of highly dispersed Pt metallic sites acting as the hydrogenation part on the catalytic reaction. Obviously, propylcyclohexanone and propylcyclohexanol disappeared after 300 min (See Table S4), indicating that the hydrogenation in the first two steps is completed within 300 min and at that point over 99% of propylcyclohexane is obtained. Finally, the high yield of propylcyclohexane (100%) was obtained at 600 min of the reaction time. To illustrate the advantage of the designed catalyst composed of metallic sites positioning close to Brønsted acid sites, the catalytic performance of ultra-small Pt nanoparticles supported on hierarchical HZSM-5 prepared via one-pot synthesis (Pt@ZSM-5NS(one)) was compared with the one obtained using Pt supported on hierarchical and conventional ZSM-5 prepared by an impregnation method (Pt@ZSM-5NS(imp), and Pt@ZSM-5CON(imp), respectively), and the Pt supported on non-acidic ZSM-5 prepared by one-pot synthesis (Pt@NaZSM-5NS(one)) (Figure 3D and Table S5).

The results show that only 41% conversion of 4-propylphenol is observed when using Pt@ZSM-5NS(imp) with 45% of propylcyclohexane selectivity, whereas 100% of 4-propylphenol conversion and propylcyclohexane selectivity is obtained when using Pt@ZSM-5NS(one). This suggests that Pt@ZSM-5NS(one) displays an outstanding and propitious catalytic performance, which might be attributed to the presence of the Lewis acid sites derived from the metallic sites of Pt, and Brønsted acid sites in zeolite framework within adjacent distance to each other.

To further elucidate the consequence of a zeolite porous system on the catalytic performance, the Pt supported on bulk HZSM-5 (Pt@ZSM-5CON(imp)) was also performed. It was found that the conversion of 4-propylphenol was only 17% with 22% of propylcyclohexane selectivity and it was significantly lower than those of Pt@ZSM-5NS(imp) as shown in Table S5. These observations clearly confirm that the presence of ultra-small Pt nanoparticles located within the adjacent distance with Brønsted acid site in the hierarchical network could improve diffusion limitation of substrates, and promoting the transfers of the intermediates between these two sites, eventually resulting in enhancing the catalytic performance of HDO process.

3. Materials and Methods

3.1. Reagent and Materials

Tetraethyl orthosilicate (TEOS: $\geq 99.0\%$, Sigma-Aldrich, St. Louis, MO, USA) was applied as a starting silica for the synthesis of silicalite-1 and ZSM-5 nanosheets. As the alumina source, aluminum isopropoxide (NaAlO_2 : $\geq 98.0\%$, Sigma-Aldrich, St. Louis, MO, USA) was utilized for hierarchical ZSM-5 and sodium aluminate (NaAlO_2 : 56 wt.% Al_2O_3 , 44 wt.% Na_2O , Riedel-deHaen, Seelze, Germany) was applied for conventional ZSM-5 zeolite. In addition, sodium hydroxide (NaOH: Carlo Erba, Barcelona, Spain) and tetra-n-butylammonium hydroxide (TBAOH: 40% in aqueous solution, LEONID, Bengaluru, India) were used as a mineralizer and a structure-directing agent (SDA), respectively. Tetrapropylammonium hydroxide solution (TPAOH: 1 M in H_2O , Sigma-Aldrich, St. Louis, Missouri, USA) has been addressed for conventional silicalite-1 and ZSM-5 as the SDA. Ammonium nitrate (NH_4NO_3 : Acros Organics, Geel, Belgium, $\geq 98\%$) was used for the ion exchange process. Tetraammineplatinum (II) nitrate ($\text{Pt}(\text{NH}_3)_4(\text{NO}_3)_2$: $\geq 99.9\%$, Sigma-Aldrich, St. Louis, MO, USA) was used as Pt source. Ethylenediamine (EDTA: $\geq 99.0\%$,

Sigma-Aldrich, St. Louis, MO, USA) was used as a ligand precursor to stabilize Pt particles. As for the hydrodeoxygenation (HDO) reaction testing, there are several reagents including 4-propylphenol ($C_9H_{11}OH$: Sigma-Aldrich, St. Louis, MO, USA), decane ($C_{10}H_{22}$: Sigma-Aldrich, St. Louis, MO, USA) and octane (C_8H_{18} : Sigma-Aldrich, St. Louis, MO, USA) as reactant, internal standard, and solvent, respectively.

3.2. Synthesis of Ultra-Small Pt Clusters Distributed on Hierarchical Silicalite-1 by a One-Pot Hydrothermal System (Pt@SiNS(one))

The ultra-small Pt nanoparticles dispersed on hierarchical siliceous nanosheets were synthesized by a basic hydrothermal process. The synthesis gel was $60SiO_2/18TBAOH/0.75NaOH/240EtOH/600H_2O/0.11Pt/0.004EDTA$ molar ratio. In a typical synthesis procedure, 8.68 g of TEOS was mixed with 0.20 g of sodium hydroxide in 2.32 mL of deionized (DI) water under vigorous stirring. Then, tetraammineplatinum (II) nitrate solution was obtained by combining 0.025 g of Pt precursor in 0.125 mL of ethylenediamine (EDTA) and 8.1 g of TBAOH under stirring at room temperature, until a homogeneous mixture was acquired. After that, the tetraammineplatinum (II) nitrate solution was added dropwise into tetraethyl orthosilicate solution. After that, it was further mixed by vigorous stirring at 25 °C for 12 h. The mixture was then transferred for the crystallization step, which is eventually heated to 403 K for 24 h. The white sediment was rinsed by DI water and the pH of the filtrate is almost neutral. Finally, the obtained samples were applied in drying process overnight at a temperature of 373 K, and calcination at 773 K for 2 h in a static air atmosphere. The sample is denoted as Pt@SiNS(one).

3.3. Synthesis of Pt on Hierarchical Silicalite-1 (Pt/SiNS(imp)) and Conventional Silicalite-1 (Pt/SiCON(imp)) by an Impregnation

The hierarchical silicalite-1 nanosheet was synthesized under hydrothermal process following literature procedure with some modifications [47,67]. The molar ratio of $60SiO_2/18TBAOH/0.75NaOH/240EtOH/600H_2O$ gel composition was prepared. Briefly, 8.6 g of TEOS was mixed with 0.02 g of NaOH, 2.32 g of DI water, and 8.10 g of TBAOH. Subsequently, it was mixed at 25 °C for 12 h. Then, the homogeneous gel was crystallized for 48 h at 403 K. The acquired powder was repeatedly washed with DI until the pH of the filtrate was almost neutral. Finally, the product was observed after drying overnight at 373 K, and calcination in air at a temperature of 773 K for 2 h.

As for the synthesis of conventional silicalite-1, the precursor of $10SiO_2/1TPAOH/1.03NaOH/240EtOH/400H_2O$ molar ratio was used. The synthesis proceeded as stated above except the hydrothermal step which was for 72 h at 453 K.

The wet impregnation of Pt on zeolite supports was performed. Typically, an aqueous solution of $Pt(NH_3)_4(NO_3)_2$ (0.6 wt.% Pt, H_2O 10 mL) was added into 1g of a zeolite support by stirring for 24 h. Subsequently, the solvent was removed for 2 h at 323 K and the achieved powder was treated under an air atmosphere at 773 K for 2 h. The sample was defined as Pt/SiNS(imp) and Pt/SiCON(imp) for Pt supported on hierarchical silicalite-1 nanosheet and conventional silicalite-1, respectively.

3.4. Synthesis of Bifunctional Catalysts (Pt@HZSM-5NS(one), Pt/HZSM-5NS(imp), and Pt/HZSM-5CON(imp))

The Pt nanoparticles supported on hierarchical HZSM-5 nanosheets gained by a hydrothermal synthesis (Pt@HZSM-5NS(one)), Pt dispersed on hierarchical surfaces of HZSM-5 nanosheets via an impregnation method (Pt/HZSM-5(imp)), and Pt on typical HZSM-5 using an impregnation method (Pt/HZSM-5CON(imp)) were prepared with the similar above-mentioned procedure as shown in Sections 3.2 and 3.3. However, in these cases, alumina sources were added in the tetraethyl orthosilicate solution mixture in order to generate aluminum sites, on which Brønsted acid sites are formed. After the calcination step to get rid of the organic template, the zeolite powder was treated with the solution of 1 M NH_4NO_3 for 2 h at 353 K with calcination in a static air atmosphere for 2 h at temperature of 773 K.

3.5. Characterization

To confirm the crystalline structure, X-ray powder diffraction (XRD) patterns were typically collected with a scan rate and a step size of 1 min^{-1} and 0.02° , respectively, on a Bruker D8 ADVANCE model (Bruker, Billerica, MA, USA). To calculate the relative crystallinity of synthesized samples, the % XRD relative crystallinity using the 2θ range of $22.5\text{--}25.0^\circ$ was obtained by $(S_x/S_r) \times 100$ and S_x and S_r correspond to the integrated peak area of the synthesized zeolite and the standard zeolite, respectively. To obtain the morphology of the samples, a JEOL-JSM-7610F and JEOL-JEM-ARM200F microscopes (Jeol Ltd., Tokyo, Japan) were utilized for scanning electron micrograph images (SEM) and transmission electron micrograph images (TEM), respectively. To observe the elemental distribution, TEM-EDS was performed. In addition, wavelength-dispersive X-ray fluorescence spectrometer (WDXRF) was used to investigate the elemental composition using Bruker model S8 TIGER sequential (Bruker, Billerica, MA, USA). The textural characteristics of all the synthesized samples were measured by a N_2 adsorption/desorption technique at the temperature of 77 K, operated on a BEL SORP MAX instrument (Bel Japan Inc., Tokyo, Japan), using the following methods: the BET, namely Brunauer-Emmett-Teller, t -plot, and BJH methods, namely Barrett-Joyner-Halenda to calculate the S_{BET} specific surface area, micropore surface area, and pore volume, together with mesopore size distribution, respectively. Ultraviolet-visible spectroscopy (UV-Vis) was performed on PerkinElmer lambda 1050 (PerkinElmer, Waltham, MA, USA) to confirm the interaction between Pt nanoparticles and thiol probe molecules. Prior to UV-Vis measurement, a zeolite was immersed in biphenyl-4-thiol solution for 1 min at room temperature. To observe the acid properties of catalysts, the ammonia temperature-programmed desorption (NH_3 -TPD) by using a BELCAT II analyzer (Bel Japan Inc., Tokyo, Japan), together with a TCD detector was performed. To study the oxidation state of Pt, X-ray absorption near-edge structure or XANES was performed by transmission mode supported by Synchrotron Light Research Institute (Public Organization), Nakhon Ratchasima, Thailand at the BL5.2 station.

3.6. Catalytic Study in Hydrodeoxygenation (HDO) of 4-Propylphenol

To demonstrate the benefit of the synthesized catalysts, the mild hydrodeoxygenation of 4-propylphenol was performed using a batch glass reactor under an atmospheric H_2 pressure with pure H_2 . Prior to reaction testing, the catalysts were dried at 373 K overnight. Subsequently, 0.10 g of sample, and 1.4 mL of 4-propylphenol was charged to the reactor together with decane and octane of 20 μL and 5 mL for an internal standard, and solvent, respectively. The highly dispersed solution was stirred at 383 K under hydrogen environment. To analyze the reaction mixture as a function of time, a gas/mass chromatography using a mass spectrometer as a detector (Agilent, GC system 7890 B, system 5977A MSD) (Agilent Technologies, Palo Alto, CA, USA) was performed. The calculated mass balance is approximately in the range of $95 \pm 2\%$.

4. Conclusions

The ultra-small Pt nanoparticles dispersed on hierarchical silicalite-1 and HZSM-5 have been effectively fabricated via a one-pot hydrothermal synthesis using ethylenediaminetetraacetic acid (EDTA) as a ligand precursor to stabilize the metals dispersed in the zeolite matrix. To demonstrate the benefits of ultra-small metal nanoparticles on a hierarchical zeolite surface as a bifunctional catalyst with respect to the one with a larger metal clusters supported on a hierarchical zeolite and the one supported on a conventional zeolite, a great catalytic behavior of almost 100% of cycloalkane product can be achieved in the consecutive mild hydrodeoxygenation (HDO) of 4-propylphenol as a model reaction under the mild condition when using the ultra-small metal nanoparticles on a hierarchical zeolite. These observations demonstrate that the presence of ultra-small Pt nanoparticles positioned at the adjacent distance with Brønsted acid site in the hierarchical structure could improve diffusion limitation of substrates, together with facilitate the intermediates between these two sites, eventually resulting in enhancing the catalytic performance. This

instance opens up perspectives to improve the efficiency of a bifunctional catalyst for bio-oil upgrading application in the biomass-derived compounds conversion to fuels.

Supplementary Materials: The following are available online at <https://www.mdpi.com/2073-4344/11/3/333/s1>, Figure S1. SEM images and particle size distribution of the synthesized Pt supported on silicalite-1 samples, Figure S2. TEM images, EDS elemental mapping for Pt on STEM images, and Pt particle size distribution of the synthesized Pt supported on silicalite-1 samples, Figure S3. XRD patterns N₂ adsorption–desorption isotherms of the synthesized bifunctional Pt supported on HZSM-5 samples, Figure S4. SEM images and particle size distribution of the synthesized bifunctional Pt supported on HZSM-5 samples, Figure S5. TEM images of the synthesized bifunctional Pt supported on HZSM-5 samples, Figure S6. Pt particle size distribution of the synthesized bifunctional Pt supported on HZSM-5 samples, Figure S7. XANES of various Pt supported zeolite samples, Figure S8. NH₃–TPD profiles of the synthesized bifunctional Pt supported on HZSM-5 samples, Table S1. Pt content and the relative crystallinity of the synthesized Pt supported on zeolites, Table S2. Textural properties of the synthesized Pt supported on HZSM-5 samples, Table S3. Summary data of the conversion and selectivity over Pt@HZSM-5NS(one) obtained at various reaction times, Table S4. Summary data of the conversion and selectivity over various catalysts.

Author Contributions: Conceptualization, S.S. and C.W.; Formal analysis, D.S., P.K., and T.W.; Investigation, P.W.; Methodology, P.W., W.W., M.K., and A.P.; Writing—original draft preparation, P.W., T.I., and S.S.; Writing—review and editing, S.S. and C.W. All authors have read and agreed to the published version of the manuscript.

Funding: This research was funded by Vidyasirimedhi Institute of Science and Technology (VISTEC). C.W. thanks the Mid-Career Research Grant 2020 from National Research Council of Thailand (NRCT5-RSA63025-03). This research also received financial support from Thailand Science Research and Innovation (TSRI) (FRB640087). In addition, this work has been partially supported by the National Nanotechnology Center (NANOTEC), NSTDA, Ministry of Science and Technology, Thailand, through its Research Network NANOTEC (RNN).

Data Availability Statement: The data presented in this study are available on request from the corresponding author.

Conflicts of Interest: The authors declare no conflict of interest.

References

1. Filho, E.P.B.; Mendoza, O.S.H.; Beicker, C.L.L.; Menezes, A.; Wen, D. Experimental investigation of a silver nanoparticle-based direct absorption solar thermal system. *Energy Convers. Manag.* **2014**, *84*, 261–267. [[CrossRef](#)]
2. Cheon, Y.E.; Suh, M.P. Multifunctional fourfold interpenetrating diamondoid network: As separation and fabrication of palladium nanoparticles. *Chem. A Eur. J.* **2008**, *14*, 3961–3967. [[CrossRef](#)]
3. Guo, J.; Zhang, J.; Gong, H.; Ju, D.; Cao, B. Au nanoparticle-functionalized 3D SnO₂ microstructures for high performance gas sensor. *Sens. Actuators B Chem.* **2016**, *226*, 266–272. [[CrossRef](#)]
4. Farka, Z.; Juřík, T.; Kovář, D.; Trnková, L.; Skládal, P. Nanoparticle-based immunochemical biosensors and assays: Recent advances and challenges. *Chem. Rev.* **2017**, *117*, 9973–10042. [[CrossRef](#)] [[PubMed](#)]
5. Sun, X.; Li, Y. Colloidal carbon spheres and their core/shell structures with noble-metal nanoparticles. *Angew. Chem.* **2004**, *116*, 607–611. [[CrossRef](#)]
6. Wang, J.; Wu, H.; Gao, D.; Miao, S.; Wang, G.; Bao, X. High-density iron nanoparticles encapsulated within nitrogen-doped carbon nanoshell as efficient oxygen electrocatalyst for zinc–air battery. *Nano Energy* **2015**, *13*, 387–396. [[CrossRef](#)]
7. Dong, C.; Lian, C.; Hu, S.; Deng, Z.; Gong, J.; Li, M.; Liu, H.; Xing, M.; Zhang, J. Size-dependent activity and selectivity of carbon dioxide photocatalytic reduction over platinum nanoparticles. *Nat. Commun.* **2018**, *9*, 1–11. [[CrossRef](#)]
8. Moliner, M.; Gabay, J.E.; Kliewer, C.E.; Carr, R.T.; Guzman, J.; Casty, G.L.; Serna, P.; Corma, A. Reversible transformation of Pt nanoparticles into single atoms inside high-silica chabazite zeolite. *J. Am. Chem. Soc.* **2016**, *138*, 15743–15750. [[CrossRef](#)]
9. Kang, J.; Cheng, K.; Zhang, L.; Zhang, Q.; Ding, J.; Hua, W.; Lou, Y.; Zhai, Q.; Wang, Y. Mesoporous zeolite-supported ruthenium nanoparticles as highly selective fischer-tropsch catalysts for the production of C₅–C₁₁ isoparaffins. *Angew. Chem. Int. Ed.* **2011**, *50*, 5200–5203. [[CrossRef](#)] [[PubMed](#)]
10. Ding, K.; Gulec, A.; Johnson, A.M.; Schweitzer, N.M.; Stucky, G.D.; Marks, L.D.; Stair, P.C. Identification of active sites in CO oxidation and water-gas shift over supported Pt catalysts. *Science* **2015**, *350*, 189–192. [[CrossRef](#)] [[PubMed](#)]
11. Li, S.; Tuel, A.; Laprune, D.; Meunier, F.; Farrusseng, D. Transition-metal nanoparticles in hollow zeolite single crystals as bifunctional and size-selective hydrogenation catalysts. *Chem. Mater.* **2015**, *27*, 276–282. [[CrossRef](#)]

12. Kim, J.; Kim, W.; Seo, Y.; Kim, J.-C.; Ryoo, R. n-Heptane hydroisomerization over Pt/MFI zeolite nanosheets: Effects of zeolite crystal thickness and platinum location. *J. Catal.* **2013**, *301*, 187–197. [[CrossRef](#)]
13. Li, X.; Chen, G.; Liu, C.; Ma, W.; Yan, B.; Zhang, J. Hydrodeoxygenation of lignin-derived bio-oil using molecular sieves supported metal catalysts: A critical review. *Renew. Sustain. Energy Rev.* **2017**, *71*, 296–308. [[CrossRef](#)]
14. Friedlander, S.K. R&D Status and Trends in Nanoparticles, Nanostructured Materials, and Nanodevices in the United States. In Proceedings of the WTEC Workshop Report, Arlington, VA, USA, 8–9 May 1997; pp. 83–88.
15. Wang, D.; Ma, B.; Wang, B.; Zhao, C.; Wu, P. One-pot synthesized hierarchical zeolite supported metal nanoparticles for highly efficient biomass conversion. *Chem. Commun.* **2015**, *51*, 15102–15105. [[CrossRef](#)]
16. Dynys, F.W.; Halloran, J.W. Influence of aggregates on sintering. *J. Am. Ceram. Soc.* **1984**, *67*, 596–601. [[CrossRef](#)]
17. Rubio-Marqués, P.; Rivero-Crespo, M.A.; Leyva-Pérez, A.; Corma, A. Well-defined noble metal single sites in zeolites as an alternative to catalysis by insoluble metal salts. *J. Am. Chem. Soc.* **2015**, *137*, 11832–11837. [[CrossRef](#)]
18. Liu, L.; Díaz, U.; Arenal, R.; Agostini, G.; Concepción, P.; Corma, A. Generation of subnanometric platinum with high stability during transformation of a 2D zeolite into 3D. *Nat. Mater.* **2017**, *16*, 132–138. [[CrossRef](#)] [[PubMed](#)]
19. Weitkamp, J.; Puppe, L. *Catalysis and Zeolites: Fundamentals and Applications*, 1st ed.; Springer: New York, NY, USA, 1999.
20. Csicsery, S.M. Shape-selective catalysis in zeolites. *Zeolites* **1984**, *4*, 202–213. [[CrossRef](#)]
21. Belaya, L.A.; Doronin, V.P.; Sorokina, T.P.; Gulyaeva, T.I. Thermal stability of zeolites Y and ZSM-5 in matrices of various compositions. *Russ. J. Appl. Chem.* **2009**, *82*, 236–242. [[CrossRef](#)]
22. Yang, Y.; Sun, C.; Du, J.; Yue, Y.; Hua, W.; Zhang, C.; Shen, W.; Xu, H. The synthesis of durable B–Al–ZSM-5 catalysts with tunable acidity for methanol to propylene reaction. *Catal. Commun.* **2012**, *24*, 44–47. [[CrossRef](#)]
23. Xue, Z.; Ma, J.; Hao, W.; Bai, X.; Kang, Y.; Liu, J.; Li, R. Synthesis and characterization of ordered mesoporous zeolite LTA with high ion exchange ability. *J. Mater. Chem.* **2012**, *22*, 2532–2538. [[CrossRef](#)]
24. Wang, N.; Sun, Q.; Bai, R.; Li, X.; Guo, G.; Yu, J. In Situ confinement of ultrasmall Pd clusters within nanosized silicalite-1 zeolite for highly efficient catalysis of hydrogen generation. *J. Am. Chem. Soc.* **2016**, *138*, 7484–7487. [[CrossRef](#)]
25. Wang, Z.; Sun, Q.; Wang, D.; Hong, Z.; Qu, Z.; Li, X. Hollow ZSM-5 zeolite encapsulated Ag nanoparticles for SO₂-resistant selective catalytic oxidation of ammonia to nitrogen. *Sep. Purif. Technol.* **2019**, *209*, 1016–1026. [[CrossRef](#)]
26. Liu, L.; Arenal, R.; Meira, D.M.; Corma, A. Generation of gold nanoclusters encapsulated in an MCM-22 zeolite for the aerobic oxidation of cyclohexane. *Chem. Commun.* **2019**, *55*, 1607–1610. [[CrossRef](#)]
27. Mohamed, E.F.; Awad, G.; Zaitan, H.; Andriantsiferana, C.; Manero, M.-H. Transition metals-incorporated zeolites as environmental catalysts for indoor air ozone decomposition. *Environ. Technol.* **2017**, *39*, 878–886. [[CrossRef](#)]
28. Farrusseng, D.; Tuel, A. Perspectives on zeolite-encapsulated metal nanoparticles and their applications in catalysis. *New J. Chem.* **2016**, *40*, 3933–3949. [[CrossRef](#)]
29. Xu, D.; Lv, H.; Liu, B. Encapsulation of metal nanoparticle catalysts within mesoporous zeolites and their enhanced catalytic performances: A Review. *Front. Chem.* **2018**, *6*, 550. [[CrossRef](#)] [[PubMed](#)]
30. Luo, W.; Cao, W.; Bruijninx, P.C.A.; Lin, L.; Wang, A.; Zhang, T. Zeolite-supported metal catalysts for selective hydrodeoxygenation of biomass-derived platform molecules. *Green Chem.* **2019**, *21*, 3744–3768. [[CrossRef](#)]
31. Munnik, P.; de Jongh, P.E.; de Jong, K.P. Recent developments in the synthesis of supported catalysts. *Chem. Rev.* **2015**, *115*, 6687–6718. [[CrossRef](#)]
32. Luo, W.; Bruijninx, P.C.; Weckhuysen, B.M. Selective, one-pot catalytic conversion of levulinic acid to pentanoic acid over Ru/H-ZSM5. *J. Catal.* **2014**, *320*, 33–41. [[CrossRef](#)]
33. Goel, S.; Wu, Z.; Zones, S.I.; Iglesia, E. Synthesis and catalytic properties of metal clusters encapsulated within small-pore (SOD, GIS, ANA) zeolites. *J. Am. Chem. Soc.* **2012**, *134*, 17688–17695. [[CrossRef](#)] [[PubMed](#)]
34. Wang, N.; Sun, Q.; Yu, J. Ultrasmall metal nanoparticles confined within crystalline nanoporous materials: A Fascinating class of nanocatalysts. *Adv. Mater.* **2019**, *31*, e1803966. [[CrossRef](#)]
35. Wang, C.; Wang, L.; Zhang, J.; Wang, H.; Lewis, J.P.; Xiao, F.-S. Product selectivity controlled by zeolite crystals in biomass hydrogenation over a palladium catalyst. *J. Am. Chem. Soc.* **2016**, *138*, 7880–7883. [[CrossRef](#)]
36. Sun, Q.; Wang, N.; Bing, Q.; Si, R.; Liu, J.; Bai, R.; Zhang, P.; Jia, M.; Yu, J. Subnanometric hybrid Pd-M(OH)₂, M = Ni, Co, clusters in zeolites as highly efficient nanocatalysts for hydrogen generation. *Chem* **2017**, *3*, 477–493. [[CrossRef](#)]
37. Zhao, M.; Yuan, K.; Wang, Y.; Li, G.; Guo, J.; Gu, L.; Hu, W.; Zhao, H.; Tang, Z. Metal-organic frameworks as selectivity regulators for hydrogenation reactions. *Nat. Cell Biol.* **2016**, *539*, 76–80. [[CrossRef](#)]
38. Goel, S.; Zones, S.I.; Iglesia, E. Encapsulation of metal clusters within MFI via interzeolite transformations and direct hydrothermal syntheses and catalytic consequences of their confinement. *J. Am. Chem. Soc.* **2014**, *136*, 15280–15290. [[CrossRef](#)] [[PubMed](#)]
39. Otto, T.; Zones, S.I.; Iglesia, E. Synthetic strategies for the encapsulation of nanoparticles of Ni, Co, and Fe oxides within crystalline microporous aluminosilicates. *Microporous Mesoporous Mater.* **2018**, *270*, 10–23. [[CrossRef](#)]
40. Cho, H.J.; Kim, D.; Li, J.; Su, D.; Xu, B. Zeolite-encapsulated Pt nanoparticles for tandem catalysis. *J. Am. Chem. Soc.* **2018**, *140*, 13514–13520. [[CrossRef](#)]
41. Wang, Y.; Wu, J.; Wang, S. Hydrodeoxygenation of bio-oil over Pt-based supported catalysts: Importance of mesopores and acidity of the support to compounds with different oxygen contents. *RSC Adv.* **2013**, *3*, 12635. [[CrossRef](#)]
42. Khan, W.; Jia, X.; Wu, Z.; Choi, J.; Yip, A.C. Incorporating hierarchy into conventional zeolites for catalytic biomass conversions: A Review. *Catalysts* **2019**, *9*, 127. [[CrossRef](#)]

43. Chen, L.-H.; Li, X.-Y.; Rooke, J.C.; Zhang, Y.-H.; Yang, X.-Y.; Tang, Y.; Xiao, F.-S.; Su, B.-L. Hierarchically structured zeolites: Synthesis, mass transport properties and applications. *J. Mater. Chem.* **2012**, *22*, 17381–17403. [[CrossRef](#)]
44. Xiao, F.-S.; Wang, L.; Yin, C.; Lin, K.; Di, Y.; Li, J.; Xu, R.; Su, D.S.; Schlögl, R.; Yokoi, T.; et al. Catalytic properties of hierarchical mesoporous zeolites templated with a mixture of small organic ammonium salts and mesoscale cationic polymers. *Angew. Chem.* **2006**, *118*, 3162–3165. [[CrossRef](#)]
45. Wang, L.; Zhang, Z.; Yin, C.; Shan, Z.; Xiao, F.-S. Hierarchical mesoporous zeolites with controllable mesoporosity templated from cationic polymers. *Microporous Mesoporous Mater.* **2010**, *131*, 58–67. [[CrossRef](#)]
46. Choi, M.; Cho, H.S.; Srivastava, R.M.; Venkatesan, C.; Choi, D.-H.; Ryoo, R. Amphiphilic organosilane-directed synthesis of crystalline zeolite with tunable mesoporosity. *Nat. Mater.* **2006**, *5*, 718–723. [[CrossRef](#)] [[PubMed](#)]
47. Chen, H.; Yang, M.; Shang, W.; Tong, Y.; Liu, B.; Han, X.; Zhang, J.; Hao, Q.; Sun, M.; Ma, X. Organosilane surfactant-directed synthesis of hierarchical ZSM-5 zeolites with improved catalytic performance in methanol-to-propylene Reaction. *Ind. Eng. Chem. Res.* **2018**, *57*, 10956–10966. [[CrossRef](#)]
48. Shetsiri, S.; Thivasasith, A.; Saenluang, K.; Wannapakdee, W.; Salakhum, S.; Wetchasat, P.; Nokbin, S.; Limtrakul, J.; Wattanakit, C. Sustainable production of ethylene from bioethanol over hierarchical ZSM-5 nanosheets. *Sustain. Energy Fuels* **2018**, *3*, 115–126. [[CrossRef](#)]
49. Luo, H.Y.; Michaelis, V.K.; Hodges, S.E.; Griffin, R.G.; Román-Leshkov, Y. One-pot synthesis of MWW zeolite nanosheets using a rationally designed organic structure-directing agent. *Chem. Sci.* **2015**, *6*, 6320–6324. [[CrossRef](#)]
50. Salakhum, S.; Saenluang, K.; Wattanakit, C. Stability of monometallic Pt and Ru supported on hierarchical HZSM-5 nanosheets for hydrodeoxygenation of lignin-derived compounds in the aqueous phase. *Sustain. Energy Fuels* **2020**, *4*, 1126–1134. [[CrossRef](#)]
51. Salakhum, S.; Yuthalekha, T.; Shetsiri, S.; Witoon, T.; Wattanakit, C. Bifunctional and bimetallic Pt–Ru/HZSM-5 nanoparticles for the mild hydrodeoxygenation of lignin-derived 4-Propylphenol. *ACS Appl. Nano Mater.* **2019**, *2*, 1053–1062. [[CrossRef](#)]
52. Kwok, K.M.; Ong, S.W.D.; Chen, L.; Zeng, H.C. Transformation of stöber silica spheres to hollow hierarchical single-crystal ZSM-5 zeolites with encapsulated metal nanocatalysts for selective catalysis. *ACS Appl. Mater. Interfaces* **2019**, *11*, 14774–14785. [[CrossRef](#)]
53. Guisnet, M. “Ideal” bifunctional catalysis over Pt-acid zeolites. *Catal. Today* **2013**, *218*, 123–134. [[CrossRef](#)]
54. Chupin, J.; Gnep, N.; Lacombe, S.; Guisnet, M. Influence of the metal and of the support on the activity and stability of bifunctional catalysts for toluene hydrogenation. *Appl. Catal. A Gen.* **2001**, *206*, 43–56. [[CrossRef](#)]
55. Blomsma, E.; Martens, J.A.; Jacobs, P.A. Isomerization and hydrocracking of heptane over bimetallic bifunctional PtPd/H-Beta and PtPd/USY zeolite catalysts. *J. Catal.* **1997**, *165*, 241–248. [[CrossRef](#)]
56. Arribas, M.; Corma, A.; Diaz-Cabañas, M.; Martínez, A. Hydrogenation and ring opening of Tetralin over bifunctional catalysts based on the new ITQ-21 zeolite. *Appl. Catal. A Gen.* **2004**, *273*, 277–286. [[CrossRef](#)]
57. Shi, Y.; Xing, E.; Wu, K.; Wang, J.; Yang, M.; Wu, Y. Recent progress on upgrading of bio-oil to hydrocarbons over metal/zeolite bifunctional catalysts. *Catal. Sci. Technol.* **2017**, *7*, 2385–2415. [[CrossRef](#)]
58. Yan, N.; Yuan, Y.; Dykeman, R.; Kou, Y.; Dyson, P.J. Hydrodeoxygenation of lignin-derived phenols into alkanes by using nanoparticle catalysts combined with Brønsted acidic ionic liquids. *Angew. Chem. Int. Ed.* **2010**, *49*, 5549–5553. [[CrossRef](#)]
59. Zhang, W.; Chen, J.; Liu, R.; Wang, S.; Chen, L.; Li, K. Hydrodeoxygenation of lignin-derived phenolic monomers and dimers to alkane fuels over bifunctional zeolite-supported metal catalysts. *ACS Sustain. Chem. Eng.* **2014**, *2*, 683–691. [[CrossRef](#)]
60. Rahman, M.; Liu, R.; Cai, J. Catalytic fast pyrolysis of biomass over zeolites for high quality bio-oil—A review. *Fuel Process. Technol.* **2018**, *180*, 32–46. [[CrossRef](#)]
61. Ohta, H.; Yamamoto, K.; Hayashi, M.; Hamasaka, G.; Uozumi, Y.; Watanabe, Y. Low temperature hydrodeoxygenation of phenols under ambient hydrogen pressure to form cyclohexanes catalysed by Pt nanoparticles supported on H-ZSM-5. *Chem. Commun.* **2015**, *51*, 17000–17003. [[CrossRef](#)] [[PubMed](#)]
62. Wannapakdee, W.; Wattanakit, C.; Paluka, V.; Yuthalekha, T.; Limtrakul, J. One-pot synthesis of novel hierarchical bifunctional Ga/HZSM-5 nanosheets for propane aromatization. *RSC Adv.* **2015**, *6*, 2875–2881. [[CrossRef](#)]
63. Yuan, E.; Wu, G.; Dai, W.; Guan, N.; Li, L. One-pot construction of Fe/ZSM-5 zeolites for the selective catalytic reduction of nitrogen oxides by ammonia. *Catal. Sci. Technol.* **2017**, *7*, 3036–3044. [[CrossRef](#)]
64. Wietecha, M.S.; Zhu, J.; Gao, G.; Wang, N.; Feng, H.; Gorring, M.L.; Kasner, M.L.; Hou, S. Platinum nanoparticles anchored on chelating group-modified graphene for methanol oxidation. *J. Power Sources* **2012**, *198*, 30–35. [[CrossRef](#)]
65. Treacy, M.M.J.; Higgins, J.B. *Collection of Simulated XRD Powder Patterns for Zeolites*, 5th ed.; Elsevier Science: Amsterdam, The Netherlands, 2007; p. 485.
66. Wang, C.; Jiang, F.; Yue, R.; Wang, H.; Du, Y. Enhanced photo-electrocatalytic performance of Pt/RGO/TiO₂ on carbon fiber towards methanol oxidation in alkaline media. *J. Solid State Electrochem.* **2013**, *18*, 515–522. [[CrossRef](#)]
67. Chen, H.; Wang, Y.; Dong, S. An effective hydrothermal route for the synthesis of multiple PDDA-protected noble-metal nanostructures. *Inorg. Chem.* **2007**, *46*, 10587–10593. [[CrossRef](#)] [[PubMed](#)]
68. Sing, K. The use of nitrogen adsorption for the characterisation of porous materials. *Colloids Surf. A Physicochem. Eng. Asp.* **2001**, *187–188*, 3–9. [[CrossRef](#)]
69. Wang, L.; Zhang, J.; Zhu, Y.; Xu, S.; Wang, C.; Bian, C.; Meng, X.; Xiao, F.-S. Strong metal–support interactions achieved by hydroxide-to-oxide support transformation for preparation of sinter-resistant gold nanoparticle catalysts. *ACS Catal.* **2017**, *7*, 7461–7465. [[CrossRef](#)]

70. Wu, G.; Zhang, N.; Dai, W.; Guan, N.; Li, L. Construction of bifunctional Co/H-ZSM-5 catalysts for the hydrodeoxygenation of stearic acid to diesel-range alkanes. *ChemSusChem* **2018**, *11*, 2179–2188. [[CrossRef](#)] [[PubMed](#)]
71. Iida, T.; Shetty, M.; Murugappan, K.; Wang, Z.; Ohara, K.; Wakihara, T.; Román-Leshkov, Y. Encapsulation of molybdenum carbide nanoclusters inside zeolite micropores enables synergistic bifunctional catalysis for anisole hydrodeoxygenation. *ACS Catal.* **2017**, *7*, 8147–8151. [[CrossRef](#)]
72. Williams, M.; Fonfe, B.; Sievers, C.; Abraham, A.; Vanbokhoven, J.; Jentys, A.; Vanveen, J.; Lercher, J. Hydrogenation of tetralin on silica–alumina-supported Pt catalysts I. Physicochemical characterization of the catalytic materials. *J. Catal.* **2007**, *251*, 485–496. [[CrossRef](#)]
73. Giovanetti, L.J.; Ramallo-López, J.M.; Foxe, M.; Jones, L.C.; Koebel, M.M.; Somorjai, G.A.; Craievich, A.F.; Salmeron, M.B.; Requejo, F.G. Shape changes of Pt nanoparticles induced by deposition on mesoporous silica. *Small* **2011**, *8*, 468–473. [[CrossRef](#)] [[PubMed](#)]
74. Short, D.; Mansour, A.; Cook, J.W., Jr.; Sayers, D.; Katzer, J. X-ray absorption edge and extended X-ray absorption fine structure studies of Pt/TiO₂ catalysts. *J. Catal.* **1983**, *82*, 299–312. [[CrossRef](#)]
75. Ichikuni, N.; Iwasawa, Y. In situ d electron density of Pt particles on supports by XANES. *Catal. Lett.* **1993**, *20*, 87–95. [[CrossRef](#)]
76. Yan, P.; Li, M.M.-J.; Kennedy, E.; Adesina, A.; Zhao, G.; Setiawan, A.; Stockenhuber, M. The role of acid and metal sites in hydrodeoxygenation of guaiacol over Ni/Beta catalysts. *Catal. Sci. Technol.* **2020**, *10*, 810–825. [[CrossRef](#)]
77. Lee, C.R.; Yoon, J.S.; Suh, Y.-W.; Choi, J.-W.; Ha, J.-M.; Suh, D.J.; Park, Y.-K. Catalytic roles of metals and supports on hydrodeoxygenation of lignin monomer guaiacol. *Catal. Commun.* **2012**, *17*, 54–58. [[CrossRef](#)]
78. Hong, D.-Y.; Miller, S.J.; Agrawal, P.K.; Jones, C.W. Hydrodeoxygenation and coupling of aqueous phenolics over bifunctional zeolite-supported metal catalysts. *Chem. Commun.* **2009**, *46*, 1038–1040. [[CrossRef](#)]
79. Wang, W.; Liu, C.-J.; Wu, W. Bifunctional catalysts for the hydroisomerization of n-alkanes: The effects of metal–acid balance and textural structure. *Catal. Sci. Technol.* **2019**, *9*, 4162–4187. [[CrossRef](#)]
80. Oh, S.; Ahn, S.-H.; Choi, J.W. Effect of different zeolite supported bifunctional catalysts for hydrodeoxygenation of waste wood bio-oil. *J. Korean Wood Sci. Technol.* **2019**, *47*, 344–359.
81. Wang, L.; Zhang, J.; Yi, X.; Zheng, A.; Deng, F.; Chen, C.; Ji, Y.; Liu, F.; Meng, X.; Xiao, F.-S. Mesoporous ZSM-5 zeolite-supported Ru nanoparticles as highly efficient catalysts for upgrading phenolic biomolecules. *ACS Catal.* **2015**, *5*, 2727–2734. [[CrossRef](#)]
82. Salakhum, S.; Yutthalekha, T.; Chareonpanich, M.; Limtrakul, J.; Wattanakit, C. Synthesis of hierarchical faujasite nanosheets from corn cob ash-derived nanosilica as efficient catalysts for hydrogenation of lignin-derived alkylphenols. *Microporous Mesoporous Mater.* **2018**, *258*, 141–150. [[CrossRef](#)]